Acta Cryst. (1988). A44, 251-257

Short-Range-Order Correlations in the Orientationally Disordered Phase of Hexachloroethane. II. Elastic and Quasielelastic Neutron Scattering

BY P. GERLACH*

Institut für Kristallographie der Universität Tübingen, Charlottenstrasse 33, D-7400 Tübingen, Federal Republic of Germany

B. DORNER

Institut Laue-Langevin, 156X, 38042 Grenoble CEDEX, France

W. PRANDL

Institut für Kristallographie der Universität Tübingen, Charlottenstrasse 33, D-7400 Tübingen, Federal Republic of Germany

AND J. LEFEBVRE

Laboratoire de Dynamique des Cristaux Moléculaires (ERA 465), Université des Sciences et Techniques de Lille I, 59655 Villeneuve d'Ascq CEDEX, France

(*Received* 21 *July* 1987; *accepted* 17 *November* 1987)

Abstract

The dynamical origin of the orientational disorder in the plastic crystalline phase of hexachloroethane (C_2Cl_6) has been determined by inelastic neutron scattering. A comparison between the energy-integrated neutron scattering and the diffuse X-ray scattering, which was reported previously, enables single-molecule scattering and contributions to the diffuse scattering due to short-range correlations to be distinguished. A single-particle rotational diffusion model explains the quasielastic part of the inelastic scattering. The one-dimensional ordered clusters have a considerably larger characteristic time and contribute to the 'elastic' intensity. Reasons for the complete absence of well defined collective translational excitations are discussed.

1. Introduction

This paper is the second part of a report about a combined X-ray and neutron scattering study of the coherent diffuse scattering in the orientationally disordered phase of hexachloroethane.

In the first part (Gerlach & Prandl, 1988, hereafter referred to as I), we analysed the diffuse X-ray scattering. We were able to distinguish between single-molecule scattering and contributions to the diffuse scattering having a more-pronounced variation of intensity due to short-range-order correlations. The single-molecule disorder is well described by a model structure which was generated in a Monte Carlo program. Steric-hindrance effects between nearest- and next-nearest-neighbour molecules determine the time-averaged orientational and centre-of-mass distribution of the individual molecule. Preferred orientations are those in which the trigonal molecular axis is parallel to the cubic body diagonals. Weaker scattering under small wave-vector transfers, in the form of (111) planes of diffuse scattering, prove in addition the existence of one-dimensional orientational correlations along the diagonals of the body-centred cubic lattice. A parallel arrangement of the trigonal axis of neighbouring molecules turned out to be energetically favourable. The intensity distribution is interpreted in terms of the Naya (1974) model, an extension of the Ising model which has two easy orientations to a system with $n > 2$ orientations.

In the present paper we investigate the dynamical origin of the disorder by analysing the energy dependence of the different parts of the diffuse scattering. Inelastic neutron scattering is a particularly powerful tool for the analysis of orientationally disordered solids (see *e.g.* Sherwood, 1979). The formalism to describe the diffuse X-ray scattering, which was developed in § 2 of paper I, can be applied in an analogous way in the analysis of the energy-integrated coherent neutron scattering, by simply replacing the $|Q|$-dependent form factor for X-rays by the constant neutron scattering length. A complication occurs, however, in the case of the Cl atoms, where the incoherent scattering is superimposed on the coherent

*Present address: Institut für Experimentalphysik der Universität Kiel, Olshausenstrasse 40, D-2300 Kiel 1, Federal Republic of Germany.

0108-7673/88/030251-07$03.00

diffuse scattering. An experimental separation of these two contributions to the scattering intensity, which was demonstrated to be feasible by polarization analysis earlier (Gerlach, Schärpf, Prandl & Dorner, 1982), could not be applied in this experiment. We will give therefore in § 3 a more qualitative description of the wavevector dependence of the elastic and inelastic coherent and incoherent scattering parts, after the description of the experimental details in § 2 of this paper. The observed single-molecule scattering is discussed in terms of a simple diffusion model in § 4 and the contribution due to short-range correlations in § 5. Finally we draw a conclusive dynamical picture of the orientational disorder in the high-temperature phase of hexachloroethane in § 6 in comparison with other related molecular crystals.

2. Experimental details

The single crystal of hexachloroethane was grown in a thin-walled cylindrical quartz-glass container by slow cooling from the melt. The crystal had a final size of about 2·5 cm^3. The mosaic spread could be improved by keeping the crystal over a long period of time at temperatures close to the melting point ($T_m = 458$ K). At the time of the experiment the mosaic spread was less than 50′.

The measurements were performed using the IN2 three-axis spectrometer at the ILL high-flux reactor at Grenoble. For most of the measurements the incident energy was fixed at 3·5 THz. Pyrolytic graphite (002) was used as monochromator and analyser. The double monochromator reduced the fast-neutron and γ background and neutrons from higher-order Bragg reflections in addition to a pyrolytic graphite filter. Collimators of 60′ before and after the monochromator and analyser gave an instrumental energy resolution of 0·26 THz (FWHM) at the elastic position. Some scans were performed with an improved resolution (0·05 THz) using an incident energy of 1·2 THz and a 30′ collimator after the monochromator together with a cooled Be filter.

Measurements of the elastic and quasielastic diffuse scattering were made using the (110) scattering plane at 413 K. Constant-Q scans were performed grouped along the lines in reciprocal space which are indicated in Fig. 1. These lines were chosen on the basis of the observed X-ray and the calculated (single-molecule) neutron scattering intensities and can be sibdivided into three groups:

(a) lines running perpendicular through the (111) planes of diffuse intensity observed in the X-ray experiment: ① and ②;

(b) lines along high-symmetry directions: *e.g.* ⟨110⟩ and ⟨001⟩, ③ and ④, respectively;

(c) lines through characteristic features of the single-molecule scattering: *e.g.* the diffuse maximum close to the forbidden 003 reflection, ④-⑦, and close to the 221 reflection, ⑧ - ⑫.

Table 1. *The scattering function and the energy-integrated scattering*

The scattering function written as a sum of a Gaussian with the instrumental energy resolution width ('elastic' part), a resolution-convoluted Lorentzian (quasielastic part) and a constant background:

$S(\mathbf{Q}, \omega) = S_{\text{elast}}(\mathbf{Q}, \omega) + S_{\text{quasi}}(\mathbf{Q}, \omega) + S_{\text{bckgr}}$

$S_{\text{elast}} = A_G R \exp[-\log 2(\omega/\Gamma_G)^2]$

$S_{\text{quasi}} = S_{\text{Lor}}(\mathbf{Q}, \omega) I^R(\omega - \omega_0)\, d\omega_0$

$S_{\text{Lor}} = A_L R \Gamma_L^2 (\omega^2 + \Gamma_L^2)$

A_G, A_L = amplitude of the Gaussian and Lorentzian, respectively

Γ_G, Γ_L = half width at half maximum of the Gaussian and Lorentzian, respectively

I^R = resolution function: Gaussian with $A_G = 1/2\Gamma_G$ and $2\Gamma_G = 0{\cdot}26$ THz, as determined with a vanadium standard

R = normalization of resolution for a constant-Q scan with constant $k_f = k_f^3 \cot\theta_A$ (Dorner, 1972)

θ_A = Bragg angle of the analyser

k_i, k_f = wavevectors of the incoming and diffracted beam, respectively

The energy-integrated scattering:

$$I_{\text{elast}}(\mathbf{Q}) = \int_{-\infty}^{+\infty} S_{\text{elast}}(\mathbf{Q}, \omega)\, d\omega = A_G 2\Gamma_G \pi^{1/2}$$

$$I_{\text{quasi}}(\mathbf{Q}) = \int_{-\infty}^{+\infty} S_{\text{quasi}}(\mathbf{Q}, \omega)\, d\omega = A_L \Gamma_L \pi$$

Strong elastic scattering, which was distributed isotropically on circles in the scattering plane, was detected at $|\mathbf{Q}| = 1{\cdot}36$, 2·74 and 3·09 Å^{-1}. The first powder ring is due to the strong 110 reflection scattered from small misaligned crystallites of hexachloroethane. The two outer rings are characterized as aluminium powder scattering from the sample holder and the furnace. All elastic contributions at these wavevector transfers were suppressed in the analysis. The quartz container could give rise to an increase in the elastic scattering at $|\mathbf{Q}| = 1{\cdot}5$ Å^{-1}, but no significant contribution was detected.

Fig. 2 shows, as an example, sequences of constant-Q scans between −2·0 and 1·0 THz recorded at Q values along the lines which are indicated in Fig. 1. All spectra are well described by an 'elastic line' sitting on a broad quasielastic distribution. The 'elastic line' displays the instrumental energy resolution, which was determined by a vanadium standard. The expression 'elastic' means that this intensity may contain true elastic scattering as well as quasielastic scattering with an energy width narrower than the experimental resolution. The quasielastic part is given by a Lorentzian, convoluted with the instrumental resolution function (for details see Table 1). The change of resolution with energy transfer leads to the asymmetry of the quasielastic line with respect to zero energy transfer visible in Fig. 2. The wavevector dependence of the quasielastic line width (FWHM = $2\Gamma_L$) obtained in a least-squares refinement and the energy-integrated elastic and quasielastic intensities

are shown for the scans ②+⑨, ③ and ④ in Figs 3(*a*)-(*c*), respectively.

3. Coherent and incoherent scattering

The total (spin plus isotopic) incoherent cross section of chlorine is $\sigma_{inc} = 5{\cdot}2 \times 10^{-28}$ m^2, the coherent cross section $\sigma_{coh} = 11{\cdot}5 \times 10^{-28}$ m^2. Adding to this the almost purely coherent cross section of the C atoms ($\sigma_{coh} = 5{\cdot}5 \times 10^{-28}$ m^2), we find that 37% of the total cross section of the hexachloroethane molecule is due to incoherent effects. A detailed analysis of the observed spectra therefore has to take into consideration both contributions. For the sake of simplicity we will discuss the general Q dependence of the coherent and incoherent scattering law in the powder average, as is shown in Fig. 4.

The broken line separates both contributions. The solid line represents the coherent diffuse scattering in the single-molecule approximation. As long as the orientational disorder is of dynamical origin, this part is purely inelastic or quasielastic. The true elastic contributions enter completely into the Bragg scattering (which is suppressed in Fig. 4). In contrast to this, the incoherent part (below the broken line) always contains an elastic and an inelastic contribution if it stems from rotational diffusion of molecules without translational diffusion. Theoretically the integral over all incoherent contributions shows no **Q** dependence. The separation into elastic and inelastic parts, which is given in Fig. 4, is calculated for a jump diffusion model (for details see Gerlach *et al.*, 1982). The elastic scattering decreases with an almost model-independent slope for $|\mathbf{Q}| < 1{\cdot}2$ Å^{-1} from the maximum in the forward scattering direction. Another maximum at about 2·6 Å^{-1} is, in comparison with the total scattering, relatively weak and is even less pronounced in more realistic stronger-disordered models.

We can therefore neglect to a good approximation elastic contributions for $|\mathbf{Q}| > 1{\cdot}3$ Å^{-1} and assume that the quasielastic incoherent scattering is constant in this region.

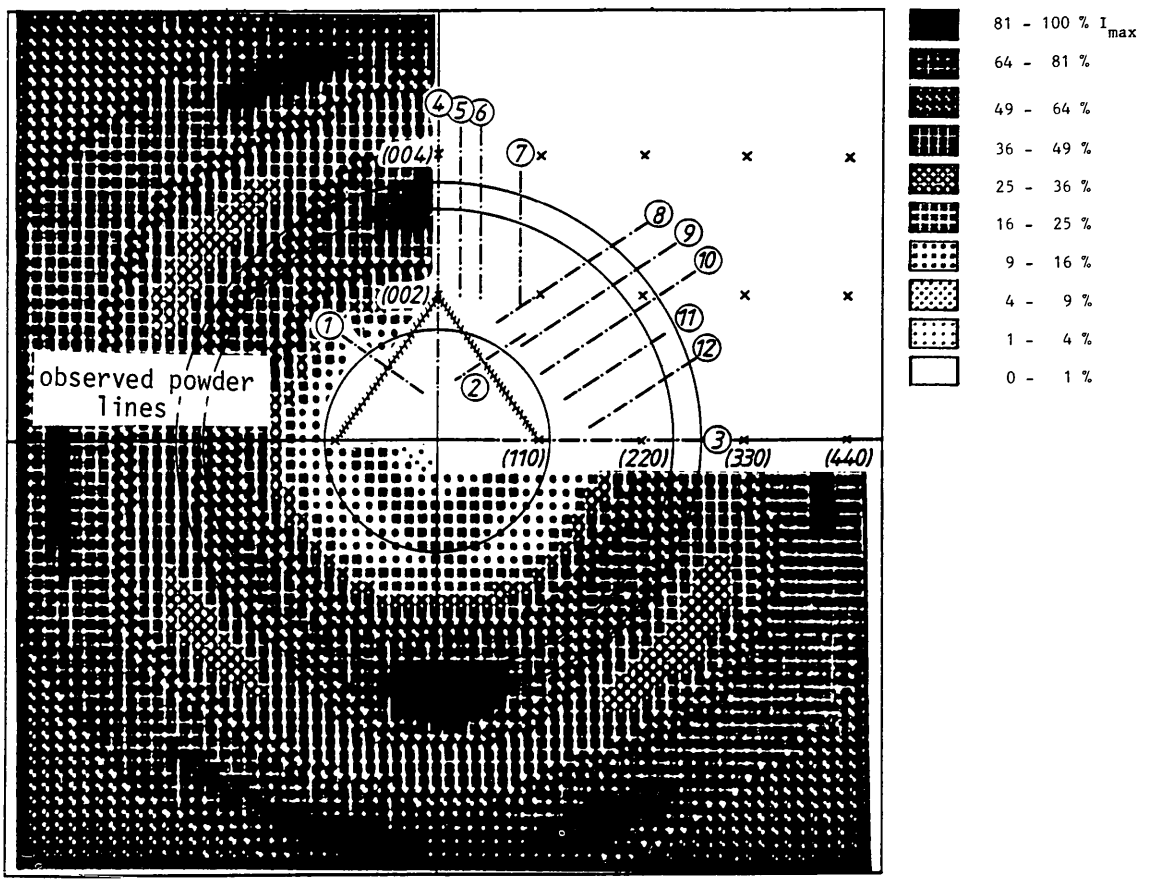

Fig. 1. The calculated single-molecule neutron scattering using the Monte Carlo routine in the (110) scattering plane. [This figure is analogous to Fig. 5(*c*) in I for X-ray scattering.] The insert shows the intensity scale using ten different grey tones. Crosses in the upper quadrant indicate the reciprocal-lattice vectors of the b.c.c. lattice given in units of $2\pi/a$. The hatched lines give the intersection of the (111) planes of diffuse intensity with the scattering plane seen in the X-ray experiment. Constant-Q scans were performed at the points along the indicated lines.

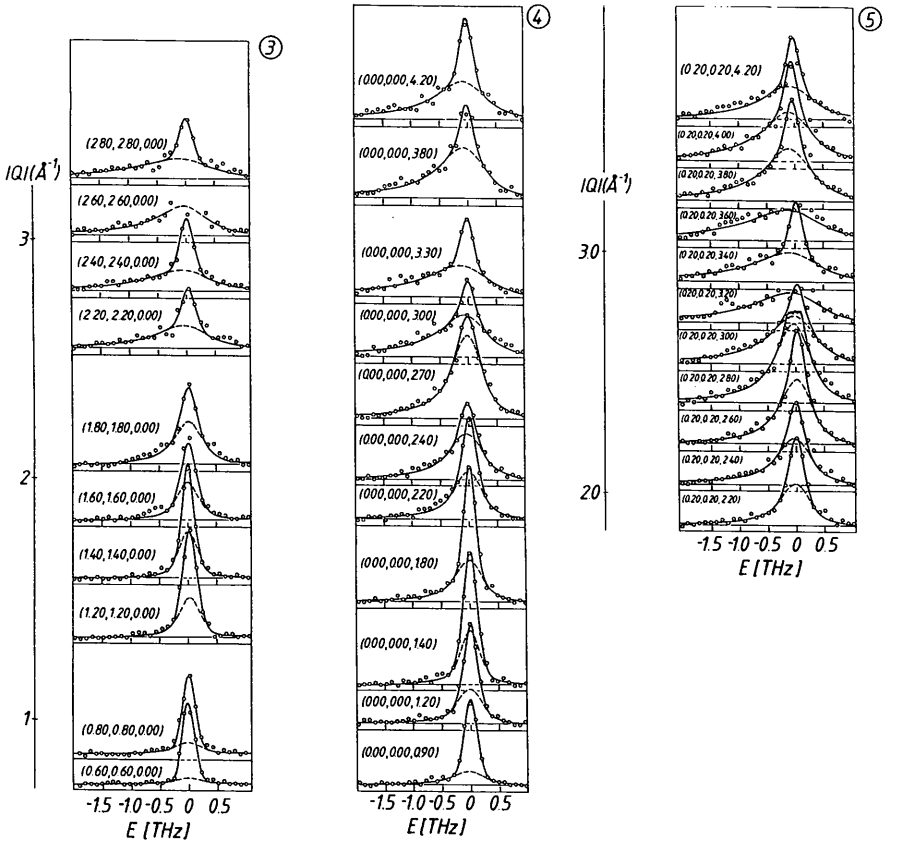

Fig. 2. Characteristic energy spectra recorded at 413 K. All intensities are given in the same arbitrary units. The numbers refer to lines given in Fig. 1. The solid line shows a fit with functions described in the text (Table 1). The broken line separates the elastic and quasielastic components.

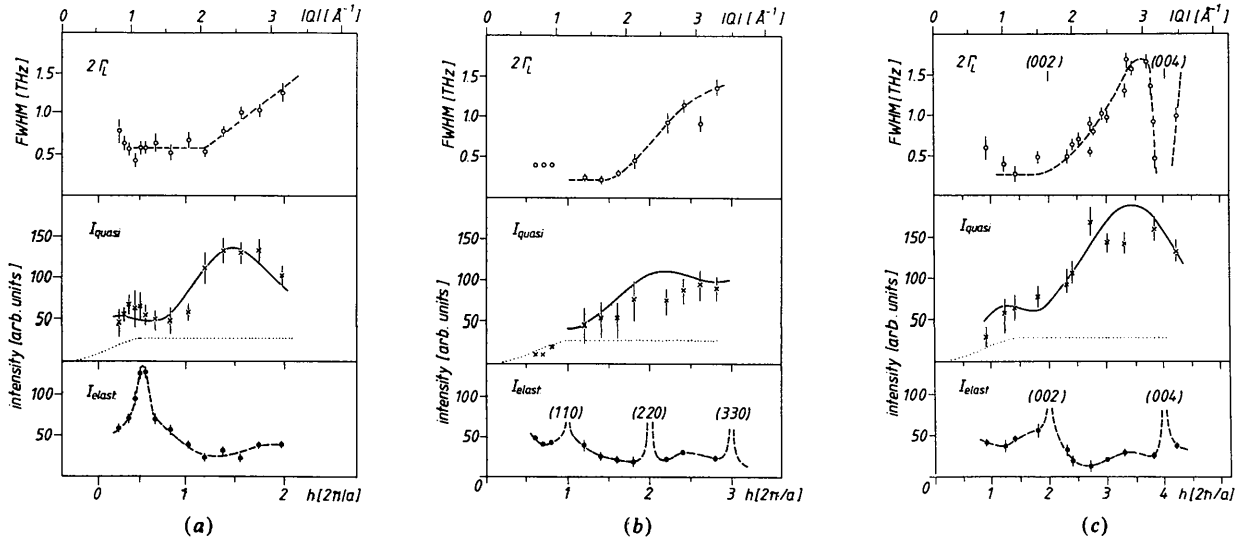

Fig. 3. Comparison of the Q dependence of the integrated quasielastic and 'elastic' scattering and the quasielastic linewidth (FWHM) along the lines given in Fig. 1. (*a*) $(h, h, h+0{\cdot}65) = ② + ⑨$; (*b*) $(h, h, 0) = ③$; (*c*) $(0, 0, h) = ④$. The solid line represents the single-molecule scattering, calculated in the Monte Carlo routine, the dotted line is the estimate of the quasielastic incoherent scattering, discussed in the text. Broken lines are only a guide to the eye. All intensities are scaled to the same arbitrary value.

It becomes clear from Fig. 4 that all inelastic contributions vanish at $Q=0$; thus we assign the forward scattering (for Q small, but away from the 000 'Bragg reflection') to purely incoherent elastic scattering. This allows in general a unique scale factor to be determined. But unfortunately we were not able to measure in the forward scattering region in this experiment, therefore we had to assume a reasonable but not absolute value for the constant quasielastic incoherent scattering at large wavevector transfers (see the dotted line in Fig. 3). Despite this remaining ambiguity and the omission of the wavevector dependence of the quasielastic incoherent scattering, several results, which are revealed by a comparison of Fig. 4 with the experimental data in Fig. 3, should be noted.

(i) The observed intensity at large wavevector transfers is in all symmetry directions predominantly quasielastic. The integral quasielastic scattering follows the Q dependence, which was calculated in the Monte Carlo routine for the single-molecule disorder scattering. The calculated intensity distribution for the coherent neutron scattering [which is analogous to Fig. 5(c) in I] is depicted in Fig. 1 and the solid lines in Fig. 3 represent details along a certain line. In particular, the anisotropy, most clearly given by the difference in the scattering between intensities measured along the $\langle hh0\rangle$ and the $\langle 00h\rangle$ directions, Figs. 3(b) and (c), respectively, is reflected in the quasielastic scattering. The related line width shows a strong increase in all symmetry directions with increasing momentum transfer.

(ii) The 'elastic' intensity has a well defined maximum under small scattering angles, where the scans ① and ② cut the (111) planes of diffuse intensity already observed in the X-ray experiment. This diffuse intensity in planes corresponds to chain-like clusters along the body diagonal. The 'elastic' scattering was compared in a series of scans in order to separate this effect from the powder scattering from misorientated crystallites. In all scans these maxima appear at slightly increased Q values, compared with Q_{110}: $Q=Q_{110}+0{\cdot}12\ (1)$ Å^{-1}.

(iii) No phonon intensities were recorded in the vicinity of the 110, 220, 211 and 222 reflections. All spectra, obtained in the constant-Q as well as the constant-E mode, were dominated by a strong quasielastic scattering, without any pronounced phonon peaks, even at small wavevector transfers $q=0{\cdot}03$ Å^{-1}. Lowering the sample temperature down to 380 K and improving the instrumental resolution (FWHM: 0·05 THz) did not change the result. The analysis of quasielastic line width showed, however, deviations from the continuous increase with increasing wavevector transfers at the high-indexed Bragg positions 004 and 222 (see, for example, Fig. 3c). We suspect that intensity contributions at low-energy transfers from unresolved acoustic phonons (or 'phonon-like' scattering) truncate the form of the single Lorentzian and lead to the fictitious line narrowing.

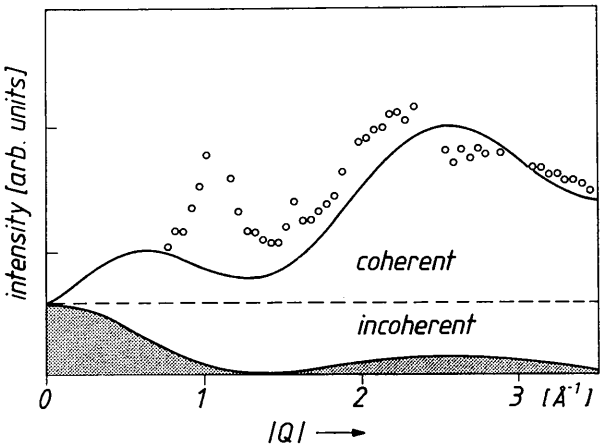

Fig. 4. Contributions to the energy-integrated diffuse scattering in the powder average. Coherent scattering: above the broken line, calculated in the single-molecule approximation. Incoherent scattering: below the broken line; the shaded area represents the elastic part in the jump model. The dots are experimental data; details are given in the text and Gerlach *et al* (1982).

4. Rotational diffusion

In the first part of this paper we demonstrated that the dominant contribution to the diffuse scattering originates from orientational disorder of the molecules. An approximative description of the single-molecule motion, which manifests itself in the quasielastic part of the energy spectrum, has to concentrate therefore on the rotational movement.

In all different symmetry directions we observe a broadening of the quasielastic linewidth with increasing wavevector. This favours a description in a diffusion-type model rather than a simple discrete jump model. The scattering function is given in the latter case by a superposition of different Lorentzians with a $|\mathbf{Q}|$-independent linewidth. In the limit of jumps between a large number of allowed equilibrium positions the scattering function becomes indistinguishable from the diffusion-type model. In the continuous diffusion model the coherent and incoherent response function is a superposition of a series of Lorentzians with increasing linewidths. The scattering law is only known explicitly for the isotropic rotational diffusion, or, in other words, for the limiting case of a vanishing angle-dependent part of the single-molecule potential (Sears, 1967; Bee, 1985). This model can serve only as a qualitative description in our case: the pronounced Q dependence of the observed diffuse scattering as well as the effective rotational potential, determined from the Bragg scattering earlier (Gerlach, Prandl & Vogt, 1984) prove

the existence of angle-dependent parts. We have to neglect this in the following. Furthermore we approximate the molecules by ideal octahedra, the C atoms being located at the centre of mass of the octahedra and not affected by the rotation. The scattering of the Cl atoms is now given, following the formalism of Sears (1967):

$$S(\mathbf{Q},\omega)=S(|\mathbf{Q}|,\omega)=\sum_{\substack{l\geq 4\\ \text{even}}} A_l T^l(\omega)+\sum_{l>0} B_l T^l(\omega);$$

coherent: $A_l \sim b_{\text{coh}}(2l+1)j_l^2(Q\rho)$;

incoherent: $B_l \sim b_{\text{inc}}(2l+1)j_l^2(Q\rho)$.

The Bessel functions j_l represent the Fourier transform of the angle-independent scattering-length-density distributions on a sphere of radius ρ.

In contrast to the incoherent part, where all functions with $l>0$ ($l=0$ is the elastic scattering) contribute to the scattering, only those functions appear in the coherent part which are totally symmetric under the transformations of the idealized molecular group $m3m$: $l=4, 6, 8$ *etc.*

The ω dependence is in both cases given by a Lorentzian of the form

$$T^l(\omega)=(\Gamma_l/\pi)/(\omega^2+\Gamma_l^2)$$

with an l-dependent width $\Gamma_l=l(l+1)D_R$, D_R being the rotational diffusion constant. Fig. 5 gives values for D_R, which were determined in a least-squares refinement of the scattering law to the experimental data in two different symmetry directions. The scattering law was convoluted with the instrumental resolution function analogous to Table 1. For wave vectors $|\mathbf{Q}|>1{\cdot}5$ Å^{-1}, the rotational constant D_R is constant: 0·018 THz. The oversimplified description in a single-molecule model is certainly no longer true at smaller wavevectors, where coherent scattering from correlated regions becomes important (compare with Fig. 5 in paper I). This explains the deviations in Fig. 5.

5. Short-range correlations

We had anticipated that short-range correlations between molecules, as far as they exist, have larger characteristic times than the single-molecule reorientations. Therefore we expected signals from correlated clusters in the 'elastic' intensity rather than in the quasielastic. The only observations are the (111) planes of diffuse scattering, where indeed the energy width could not be resolved. Therefore we can only give a lower limit for the lifetime of these chain-like clusters: $\tau>4{\cdot}8\times10^{-11}$ s. We searched very carefully for (222) planes without success. The energy width of this diffuse scattering should be the same as for the (111) planes.

6. Concluding remarks

The present X-ray and inelastic neutron study demonstrates that the orientational disorder in the high-temperature phase of hexachloroethane is predominantly a single-particle phenomenon of dynamical origin. The molecules perform uncorrelated large-amplitude librational motions around a number of equilibrium orientations. The equilibrium orientations are determined by short-range interactions (steric hindrance) with the nearest- and next-nearest-neighbour molecules. The absence of well defined modes in the inelastic spectra prove these motions as overdamped and of relaxational character. The librations are frequently interrupted by jumps between symmetry-related equilibrium orientations; these were detected earlier by the analysis of the incoherent scattering (Gerlach *et al.*, 1982). A description of this complex type of motion in terms of a simplified isotropic rotational diffusion model gives the diffusion constant $D_R=0{\cdot}018$ THz.

From the single-molecule point of view, hexachloroethane satisfies the requirement for the concept of orientational frustration (Dove & Pawley, 1984); the librational motion causes the sites - distinct only through the small distortion of the molecule from the octahedral shape - to appear equivalent. For such systems, in which the crystal site and molecular symmetry are identical, the frustration model explains the orientational disorder as a result of the 'ordering' due to nearest-neighbour and 'disordering' due to next-nearest-neighbour interactions. This leads to the observed large-amplitude librations and reorientational jumps. In addition to this we were able to identify one-dimensional clusters of short-range-ordered molecules. These precursor orientational ordering effects are new for the class of ODIC crystals build up from octahedral or almost octahedral molecules [but were reported earlier in the case of CBr_4 (More, Lefebvre & Hennion, 1984)]. No such effects were detected, for example in SF_6, where this conclusion was drawn, however, by inspecting the

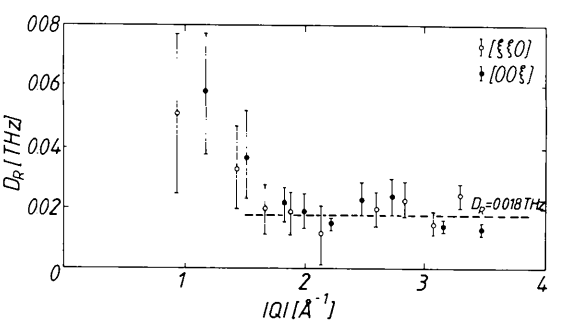

Fig. 5. The rotational diffusion constant D_R determined in a refinement of the Lorentzian linewidth in the isotropic rotational diffusion model at different wavevectors along the lines ③ (open circles) and ④ (closed circles) of Fig. 1.

time-dependent molecular trajectories calculated in a molecular dynamics study (Dove, Fincham & Hubbard, 1986); a detailed study of the diffuse scattering from a single crystal of SF_6 is still missing.

The occurrence of the maxima of diffuse intensity in C_2Cl_6 at wavevectors slightly larger than the (111) planes in reciprocal space might be a hint to a rotational-translational coupling connected with the orientational ordering: the attractive forces between two parallel orientated nearest-neighbour molecules cause a decrease in the centre-of-mass distance of about 8%.

A remarkable experimental fact is the complete absence of well defined collective translational excitations. While it is well known that librational modes are usually overdamped in ODIC phases of molecular crystals, it is surprising that no acoustic modes could be resolved, even at small wavevector transfers. It is difficult experimentally to extend the investigation closer to the Brillouin-zone centre, because elastic scattering from misaligned crystallites leads to spurious peaks in this region. The analysis of the energy-integrated scattering has shown that the thermal diffuse scattering due to phonons is relatively weak in comparison with the orientational disorder scattering. This suggests that the translational displacements are also of overdamped character probably due to a strong translational-rotational coupling. SF_6 is another example where a similar measurement (Dove, Pawley, Dolling & Powell, 1986) revealed no well defined acoustic modes, in contrast to most other orientationally disordered crystals (*e.g.* CD_4, CBr_4, N_2) in which the acoustic phonons are well defined, at least at small wavevectors.

References

BEE, M. (1985). *J. Chim. Phys. Phys. Chim. Biol.* **82**, 205-218.

DORNER, B. (1972). *Acta Cryst.* A**28**, 319-327.

DOVE, M. T., FINCHAM, D. R. & HUBBARD, R. E. (1986). *J. Mol. Graphics*, **4**, 79-81.

DOVE, M. T. & PAWLEY, G. S. (1984). *J. Phys. C*, **17**, 6581-6599.

DOVE, M. T., PAWLEY, G. S., DOLLING, G. & POWELL, B. M. (1986). *Mol. Phys.* **57**, 865-880.

GERLACH, P. & PRANDL, W. (1988). *Acta Cryst.* A**44**, 128-135.

GERLACH, P., PRANDL, W. & VOGT, K. (1984). *Mol. Phys.* **52**, 383-397.

GERLACH, P., SCHÄRPF, O., PRANDL, W. & DORNER, B. (1982). *J. Phys.* **43**, 151-157.

MORE, M., LEFEBVRE, J. & HENNION, B. (1984). *J. Phys. (Paris)*, **45**, 303-307.

NAYA, S. (1974). *J. Phys. Soc. Jpn*, **37**, 340-347.

SEARS, V. F. (1967). *Can. J. Phys.* **45**, 237-254.

SHERWOOD, J. N. (1979). Editor. *The Plastically Crystalline State.* New York: John Wiley.

Acta Cryst. (1988). A**44**, 257-262

A General Lorentz Correction for Single-Crystal Diffractometers

BY G. J. MCINTYRE* AND R. F. D. STANSFIELD†

Institut Laue-Langevin, 156*X*, 38042 *Grenoble CEDEX, France*

(*Received* 18 *June* 1987; *accepted* 19 *November* 1987)

Abstract

A single-crystal Lorentz correction is derived for the case of a general scan through an out-of-plane reflection on a four-circle diffractometer with relaxed sample-to-detector collimation. When the Lorentz correction is expressed in terms of the incremental steps in the Eulerian setting angles, structure amplitudes observed by different scan trajectories, for example, some angular in real space and others linear in reciprocal space, are put on a common scale, and errors due to known missetting of the angles or rounding off of the angles are avoided.

Introduction

In a conventional single-crystal diffraction experiment the integrated intensities of the reflections are measured by rotation of the crystal about one axis of the diffractometer, usually that axis which best resolves neighbouring reflections. For a constant velocity of rotation of the crystal, different reciprocal-lattice points pass through the Ewald sphere at different rates and therefore have different times-of-reflection opportunity. The inverse of the correction factor to be applied to the observed integrated intensities to obtain (relative) squared structure amplitudes is called the Lorentz factor, following the demonstration of its dependence on the experimental arrangement by Lorentz in one of his classroom lectures (Azaroff, 1968).

For some structures, particularly those which are incommensurate or exhibit macroscopic stacking

*Present address: The Studsvik Neutron Research Laboratory, University of Uppsala, S-61182 Nyköping, Sweden.

†Present address: Department of Biochemistry, University of Edinburgh, Hugh Robson Building, George Square, Edinburgh EH8 9XD, Scotland.

0108-7673/88/030257-06$03.00